ARTICLE

Fluorinated Phenoxy Boron Subphthalocyanines in Organic Light-Emitting Diodes

Graham E. Morse,[†] Michael G. Helander,[‡] Jozef F. Maka,[†] Zheng-Hong Lu,[‡] and Timothy P. Bender*[,†]

Department of Chemical Engineering and Applied Chemistry, University of Toronto, 200 College Street, Toronto, Ontario M5S 3E5 Canada, and Department of Material Science and Engineering, University of Toronto, 184 College Street, Toronto, Ontario M5S 3E4, Canada

ABSTRACT Three fluorinated **BsubPc**s have been synthesized and characterized. Crystals suitable for XRD were grown by slow vapor diffusion and sublimation. Analysis of their crystal structures revealed a dimeric association of **BsubPc** units for **F_5BsubPc** and columnar packing for **F_{12}BsubPc** and **F_{17}BsubPc**. Cyclic volatmmetry (CV) was used to probe the frontier orbital energy levels of these compounds in both dichloromethane and acetonitrile solution; however, only **F_5BsubPc** underwent oxidative events, whereas all three compounds underwent reductive events. A −362 and −37 mV shift in the reductive peak potential was observed for peripheral and axial fluorination, respectively, as measured by cyclic voltammetry. Solution UV−vis absorption and photoluminescence spectra were measured in dichloromethane. All three compounds demonstrated air-stable *n*-type conductivity in single-carrier devices and extremely narrow orange EL emission with a fwhm of only ∼30 nm. **F_5BsubPc** showed a maximum luminescence of 122 cd/m^2 at 8 V, with a maximum current efficiency of 0.03 cd/A, whereas the devices fabricated from **F_{12}BsubPc** and **F_{17}BsubPc** produced luminescence with a maximum value of <1 cd/m^2.

KEYWORDS: organic • light-emitting diode • boron • subphthalocyanine • electronic fluorination

INTRODUCTION

Boron subphthalocyanine (**BsubPc**) is the only known lower direct analog of a more general class of compounds the metal phthalocyanines (**Pc**s). It is formed exclusively by heating of phthalonitrile in the presence of a boron template (BCl_3 or BBr_3). After the initial discovery of Cl-**BsubPc** (1) some 30 years ago, the understanding of the chemistry and properties of Cl-**BsubPc** were expanded upon by Kobayashi (2), who showed that Cl-**BsubPc** and its derivatives could undergo a ring-expansion reaction to give asymmetric **Pc**s. Since the turn of the millennium (3), Torres et al. (4) reported a simplified synthesis and purification of Cl-**BsubPc** from BCl_3 and phthalonitrile and deduced the mechanism of its formation (5). His research group now uses **BsubPc** as a building block for molecular electronic devices and supramolecular assemblies (6). The highly conjugated aromatic system of **BsubPc** and its unique bowl-shaped structure (Figure 1) has seen it attract attention for a variety of optoelectronic applications, including as a solution-processable fluorescent dopant emitter (7) and vacuum sublimable hole injection layer (8) in organic light-emitting diodes (OLEDs), as well as an active component in thin film solar cells (9). In the reports concerning devices made by vacuum sublimation (9a–9f), the **BsubPc** derivative used generally retains the hydrolytically unstable B−Cl moiety present in the most common form Cl-**BsubPc**, or in one case has been replaced with a B−F (9c). The longevity of an electronic device obviously depends on the stability of the material on the molecular level in particular toward oxygen and moisture. Relevant to **BsubPc**s, the boron−halogen bonds (either B−Cl or B−F) are reactive with water, producing either B−OH or the dehydrated μ-oxo (B−O−B) dimeric species. Although water can be excluded from OLEDs and organic solar cells by encapsulation, this technique adds significant cost to the resulting devices. As such, we wish to answer the question of whether useful **BsubPc** derivatives can be made that do not contain the hydrolytically unstable B−Cl or B−F moieties but rather the more hydrolytically stable B−O bond. Such bonding motifs can be formed by facile displacement of the halogen of Cl-**BsubPc** derivatives with a variety of phenols yielding phenoxy-**BsubPc**s (4). Doing so obviously adds significant mass to the resulting **BsubPc** derivatives, potentially making vacuum sublimation problematic. On the positive side, structural variables would be available through the use of the plethora of commercially available phenols and such structural variations could make possible the control of the **BsubPc** molecular arrangement in the resulting vacuum-deposited thin solid films.

We wish to report the synthesis and characterization of a series of three structurally related fluorinated phenoxy-**BsubPc**s that contain hydrolytically stable B−O bonds (Scheme 1). We have termed these compounds **F_5BsubPc**,

* To whom correspondence should be addressed. E-mail: tim.bender@utoronto.ca.

Received for review March 24, 2010 and accepted June 4, 2010

† Department of Chemical Engineering and Applied Chemistry, University of Toronto.

‡ Department of Material Science and Engineering, University of Toronto.

DOI: 10.1021/am1002603

Published on Web 06/22/2010

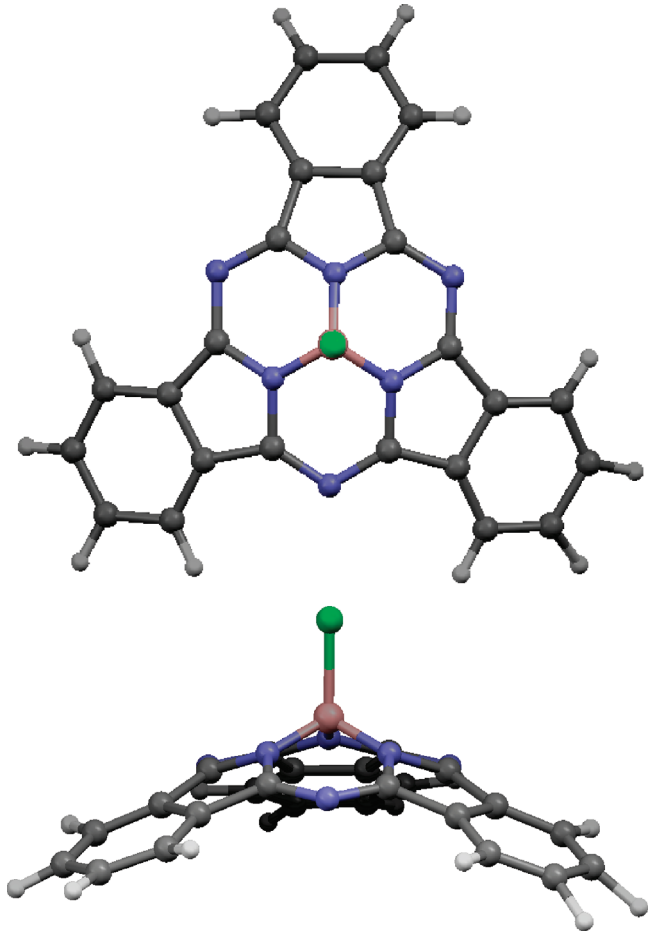

FIGURE 1. Cl-BsubPc in its single crystal viewed from the top (top) and side (bottom, carbon, gray; nitrogen, blue; boron, brown; chlorine, green). Image produced using Mercury Viewer using X-ray diffraction data extracted from the CCD (25a).

F_{12}BsubPc, and **F_{17}BsubPc**, in each case indicating the total amount of fluorine present within the **BsubPc** derivative. Within this series, **F_{12}BsubPc** is known (10), whereas **F_5BsubPc** and **F_{17}BsubPc** are novel. The sum of this series of **BsubPc** derivatives contains systematic variations in the amount and positioning of fluorine atoms within the chemical structure, thereby making the formation of structure property relationships possible. We have targeted fluorinated **BsubPc** derivatives due to the known thermal stability and nonassociative nature of fluorinated organic groups in the solid state (11). As a result, even though we have increased the mass of the **BsubPc** derivatives, we have maintained the ability to sublime then into thin solid films. **F_5BsubPc** is derived from Cl-**BsubPc** (12), whereas **F_{12}BsubPc** and **F_{17}BsubPc** are derived from Br-**F_{12}BsubPc** (13). The presence of fluorine around the periphery of the latter two compounds is known to affect the position of the respective HOMO and LUMO compared to the hydrogenated counterpart (6b). Each of **F_5BsubPc**, **F_{12}BsubPc**, and **F_{17}BsubPc** are sublimable and has been incorporated into a variety of active layers of OLED devices through ultrahigh vacuum deposition without encapsulation. We have found that depending on the molecular structure, each **BsubPc** has an optimal role within the resulting OLED device and we have therefore formed structure property relationships within these three compounds.

Scheme 1. Synthesis of (a) F_5BsubPc from Cl-BsubPc and Both (b) F_{12}BsubPc and F_{17}BsubPc from Br−F_{12}BsubPc

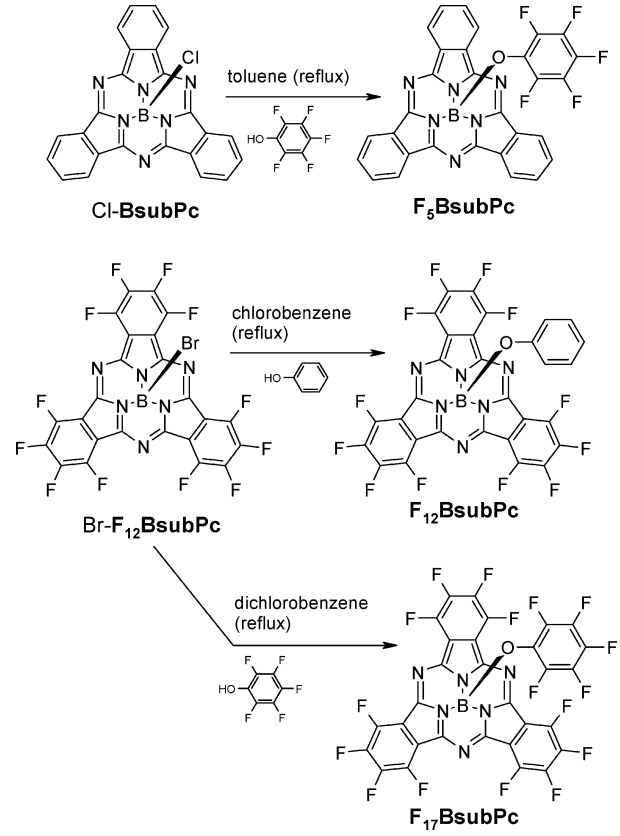

EXPERIMENTAL SECTION

Methods and Materials. All solvents were purchased from Caledon Laboratories Ltd. (Caledon, Ontario, Canada) and used as received unless stated otherwise. 1,2-Dichlorobenzene was purchased from TCI America and used as received. Chromatography (Kaufmann and flash) was performed using 50−100 μm silica gel which was purchased from Caledon Laboratories Ltd. (Caledon, Ontario, Canada) and used as received. Thin film chromatography (TLC) was performed using Alugram a 40 × 80 mm 0.2 mm thick silica gel on an aluminum substrate with fluorescence indicator supplied by Macherey-Nagel through Caledon Laboratories Ltd. (Caledon, Ontario, Canada). Soxhlet extractions were performed using Whatman single thickness cellulose extraction thimbles (33 × 118 mm). All nuclear magnetic resonance (NMR) spectra were acquired on a Varian Mercury 400 MHz system in deuterated chloroform ($CDCl_3$) purchased from Cambridge Isotope Laboratories which was used as received. All ^{1}H NMR spectra where referenced to an internal standard of 0.05% TMS. All ^{19}F spectra were referenced to an external standard (present as a concentric tube) of $BF_3 \cdot O(C_2H_5)_2$. All crystal structures were collected using computer-controlled KappaCCD system and an Oxford Cryostream variable temperature apparatus. Ring centroid proximities were calculated/measured by using PLATON (14). All ultraviolet−visible (UV−vis) spectroscopy was performed using PerkinElmer Lambda 25 in a PerkinElmer quartz cuvette with a 10 mm path length for solution phase samples and on polished quartz wafers supplied by Ted Pella for thin film samples. Photoluminescence spectra were collected using a Perkin-Elmer LS 55. All Fourier

transform infrared spectroscopy (FT-IR) was run on KBr disks in a Perkin-Elmer Spectrum 100. High pressure liquid chromatography (HPLC) analysis was conducted using a Waters 2695 separation module with a Waters 2998 photodiode array and a Waters 4.6 mm × 100 mm SunFire C_{18} 3.5 μm column. HPLC grade acetonitrile (ACN) purchased from Caledon Laboratories Ltd. (Caledon, Ontario, Canada) was eluted at 0.6 mL/min during operation. Cyclic voltammetry was performed with a Bioanalytical Systems C3 electrochemical workstation. The working electrode was a 1 mm platinum disk with a platinum wire used as a counter electrode. The reference electrode was $Ag/AgCl_2$ saturated salt solution. All electrochemistry was done in spec-grade solvents as indicated (Caledon Laboratories, Caledon, Ontario, Canada). The solvents were purged with Argon at room temperature prior to use. Three cycles from +1.6 to −1.6 V were measured for each compound at a scan rate of 100 mV/s. Decamethylferrocene was used as an internal reference. The half-wave reduction potential ($E_{1/2,red}$) of decamethylferrocene was previously measured to be −0.012 V vs $Ag/AgCl_2$ by comparison to *N*,*N*′-diphenyl-*N*,*N*′-bis(3-methylphenyl)-[1,1′-biphenyl]-4,4′-diamine (TPD), which has an established first half-wave oxidation potential ($E^1_{1/2,ox}$) of 0.805 V vs Ag/AgCl (15). Melting points were measured using a Stuart SMP3 melting point apparatus. Schematics and instructions for use for both the Kauffman column chromatography and train sublimation apparatus are given in the Supporting Information accompanying this article. Mass spectrometry was performed on a Waters GC time-of-flight mass spectrometer with an electron ionization probe and accurate mass determination. Carbon/hydrogen/nitrogen elemental analysis was performed using a Perkin-Elmer 2400 Series II CHNS Analyzer.

Chloroboronsubphthalocyanine (Cl-BsubPc). Cl-**BsubPc** was synthesized as previously report (16) by adapting a published procedure (12). Phthalonitrile (5.32 g, 2.4 × 10^{-2} mol) was dissolved with stirring in 1,2-dichlorobenzene (220 mL) in a round-bottomed flask fitted with a short path distillation column and placed under a constant flow of argon gas toward the short path distillation column. To this solution BCl_3 was added (100 mL of 1.0 M solution (0.1 mol) in heptane) in a single portion. On gradual heating, the heptane was distilled off. When distillation was complete, the reaction was heated at reflux for an additional 1.5 h. After cooling, the solvent was removed by rotary evaporation. The resulting crude product was extracted with hot methanol in a Soxhlet extraction apparatus for 8 h. The resulting golden-brown powder was then rinsed with diethyl ether and dried in the vacuum oven. We have achieved typical yields of 3.5−4.3 g (59−72%) in our laboratory. ^{1}H NMR (400 MHz, $CDCl_3$, Me_4Si): δ 7.95−7.97 (6 H, m), 8.90−8.92 (6 H, m).

Bromododecafluoroboronsubphthalocyanine (Br-F_{12}BsubPc). (Br-**F_{12}BsubPc**) was synthesized by adapting the method of Sharman (13). We found the reported method was not satisfactory to reliably produce large quantities of pure Br-**F_{12}BsubPc** as produced samples typically contained 28% tetrafluorophthalmide. The method used to confirm the presence of tetrafluorophthalimide is outlined below. The following is the adapted procedure with yields given as ranges over 4 runs. Chlorobenzene (21 mL) was added to tetrafluorophthalonitrile (6.07 g, 3.0 × 10^{-2} mol) in a 100 mL three-neck, round-bottom flask. To this BBr_3 was slowly added to the flask (neat, 2 mL, 2.1 × 10^{-2} mol) to the flask. The mixture was then heated to 100 °C for 4 h, cooled to room temperature, and the solvent and any remaining BBr_3 was removed by rotary evaporation yielding a mass of crude product (9.1 − 9.4 g). The crude product was purified by Kauffman column chromatography using silica gel as the absorbent and dichloromethane as the eluent. After being cooled, the dichloromethane was removed by rotary evaporation, yielding Br-**F_{12}BsubPc** (Yield 2.9−3.4 g, 93−96% purity by HPLC maxplot, the remaining 7−4% being tetrafluorophthalimide). Structural confirmation of Br-**F_{12}BsubPc** could be accomplished using ^{19}F NMR:^{19}F NMR (400 MHz, $CDCl_3$, $BF_3 \cdot O(C_2H_5)_2$): δ 6.66 to 6.73 (6F, q), 17.11 to 17.18 (6F, q). Br-**F_{12}BsubPc** was used without further purification in the subsequent steps. Single crystals of Br-**F_{12}BsubPc** of suitable quality for X-ray diffraction were grown by slow vapor diffusion of heptane into benzene allowing for further structural confirmation. For reference, a pure sample of tetrafluorophthalimide was isolated by washing the post-Kauffman column mass with water (tetrafluorophthalimide being extracted into the water). Single crystals of tetrafluorophthalimide were obtained by slow evaporation of the water and its structure confirmed by diffraction of those crystals. A thermal ellipsoid plot of the isolated tetrafluorophthalimide is given in the Supporting Information. Additional structural confirmation of tetrafluorophthalimide was provided using ^{19}F NMR and FT-IR. ^{19}F NMR (400 MHz, $CDCl_3$, $BF_3 \cdot O(C_2H_5)_2$): δ 11.83 to 11.91 (2F, q), 18.32 to 18.40 (2F, q). FT-IR (KBr, cm^{-1}): 2985 υ(strong); 2891 υ(weak); 1775 υ(weak); 1723 υ(C═O, strong); 1512, 1502 (medium); 1382 υ(broad, medium); 1250 υ(weak); 1160 υ(weak); 1061 υ(weak); 1043 υ(medium); 956 υ(broad, weak); 927 υ(weak).

Pentafluorophenoxyboronsubphthalocyanine (F_5BsubPc). Cl-**BsubPc** (1.0 g, 2.3 × 10^{-3} mol) was combined with pentafluorophenol (2.2 g, 1.2 × 10^{-2} mol) and toluene (10 mL) in a 50 mL round-bottom flask fitted with a condenser and held under a constant pressure of argon gas. The reactants were heated at reflux (∼111 °C) for 16 h, at which time the reaction was confirmed to be complete by HPLC analysis (absence of Cl-**BsubPc**) and was subsequently cooled to room temperature. The toluene was removed by rotary evaporation, yielding crude product (2.3 g, a mixture of **F_5BsubPc**, residual tetrafluorophthalimide and excess pentafluorophenol as confirmed by HPLC analysis). The crude product was purified using Kauffman column chromatography with basic alumina and dichloromethane as the eluent. Removal of the dichloromethane by rotary evaporation yielded a mass of 1.5 g (93% **F_5BsubPc** with the balance tetrafluorophthalimide and trace pentafluorophenol by HPLC maxplot). Subsequently the mass (750 mg) was further purified using train sublimation. The apparatus was operated under a vacuum with a controlled flow of nitrogen gas generating an internal pressure of 1 × 10^{-1} Torr. The temperature was increase from room temperature to 300 °C over a period of 4 h and held constant for 2 h and then allowed to cool back to room temperature. The fastest running band was confirmed as **F_5BsubPc** and had the appearance of a metallic gold film (yield 440 mg, 7.6 × 10^{-4} mol, 59% yield from mass placed in the train sublimation apparatus, >99.9% purity). ^{1}H NMR (400 MHz, $CDCl_3$, Me_4Si): δ 7.92 to 7.97 (6 H, m), 8.85 to 8.90 (6 H, m). ^{19}F NMR (400 MHz, $CDCl_3$, $BF_3 \cdot O(C_2H_5)_2$): δ −5.57 to −5.63 (2F, d), −10.80 to −10.90 (2F, t), −11.74 to −11.86 (1F, t), mp 280 °C. Anal. Calcd for $C_{30}H_{12}N_6OF_5B$: C, 62.31; H, 2.09; N, 14.53. Found: C, 62.14; H, 2.34; N, 14.49. HRMS (positive) exact mass calcd for $C_{30}H_{12}N_6OF_5B$, 578.1086; found, 578.1093. Crystals of suitable quantity for X-ray diffraction were grown by slow vapor diffusion of heptane into a benzene solution.

Phenoxydodecafluoroboronsubphthalocyanine (F_{12}BsubPc). Br-**F_{12}BsubPc** (1.0 g, 1.4 × 10^{-3} mol) was combined with phenol (0.7 g, 7.4 × 10^{-3} mol) and dichlorobenzene (10 mL) in a 25 mL round-bottom flask fitted with a condenser and held under a constant pressure of argon gas. The contents were heated at reflux (∼180 °C) for 20 h. The completion of the reaction was confirmed by HPLC (absence of Br-**F_{12}BsubPc**) the reaction was let to cool to room temperature. The solvent was removed by rotary evaporation. The crude product was purified using Kauffman column chromatography with silica gel and dichloromethane as the eluent. Removal of the dichloromethane by rotary evaporation yielded a mass of 0.792 g (94% **F_{12}BsubPc** with the balance tetrafluorophthalimide and trace phenol by HPLC maxplot). Subsequently, part of the mass (680 mg) was further purified by train sublimation. The temperature was

periodically increased from room temperature up to 410 °C over a period of 4 h, held constant for 2 h, and then allowed to cool to room temperature. The slowest running band was identified as **F_{12}BsubPc**, which appeared as a metallic gold film (yield 350 mg, 5.0×10^{-4} mol, 52% yield from mass placed in the train sublimation apparatus, >99.9% pure). ^{1}H NMR (400 MHz, $CDCl_3$, Me_4Si): δ 5.33 to 5.38 (2H, d), 6.68 to 6.73 (1H, t), 6.78 to 6.84 (2H, t). ^{19}F NMR (400 MHz, $CDCl_3$, $BF_3 \cdot O(C_2H_5)_2$): δ 5.50 to 5.56 (6F, q), 16.19 to 16.26 (6F, q). Mp 342 °C. Anal. Calcd for $C_{30}H_5N_6OF_{12}B$: C, 51.17; H, 0.72; N, 11.93. Found: C, 50.60; H, 0.87; N, 11.97. HRMS (positive) exact mass calcd for $C_{30}H_5N_6OF_{12}B$, 704.0426; found, 704.0433. Crystals of suitable quantity for X-ray diffraction were grown by slow vapor diffusion of heptane into a benzene solution.

Pentafluorophenoxydodecafluoroboronsubphthalocyanine (F_{17}BsubPc). Br-**F_{12}BsubPc** (4.5 g, 4.3×10^{-3} mol) was combined with pentafluorophenol (4.0 g, 2.2×10^{-2} mol) and toluene (30 mL) in a 100 mL rounded bottom flask fitted with a condenser and held under a constant pressure of argon gas. The reactants were heated at reflux (~111 °C) for 50 h. The reaction was monitored and confirmed complete by HPLC (absence of Br-**F_{12}BsubPc**). The reaction was cooled to room temperature and the solvent removed by rotary evaporation. The crude product was purified using Kauffman column chromatography with silica gel and dichloromethane as the eluent. Removal of the dichloromethane by rotary evaporation yielded a mass of 4.7 g (95% **F_{17}BsubPc** with the balance tetrafluorophthalimide, trace pentafluorophenol, and other unidentifiable impurities (HPLC maxplot)). Further purification was deemed necessary. Part of the mass (2.0 g) was subsequently purified by flash chromatography on silica using dichloromethane as the eluent. The dichloromethane was removed by rotary evaporation and the resulting mass (501 mg, 25% yield) was train sublimed. The temperature was increase from room temperature to 350 °C over a period of 4 h, held constant for an additional 2 h then cooled to room temperature. The fastest running band was identified as **F_{17}BsubPc** and appeared as a metallic gold film (yield 275 mg, 3.5×10^{-4} mol, 55% yield based on amount loaded into the train sublimation apparatus, 99.6% pure by HPLC maxplot). ^{1}H NMR (400 MHz, $CDCl_3$, Me_4Si): δ 5.33 to 5.38 (2H, d), 6.68 to 6.73 (1H, t), 6.78 to 6.84 (2H, t). ^{19}F NMR (400 MHz, $CDCl_3$, $BF_3 \cdot O(C_2H_5)_2$): δ −9.52 to −9.41 (1F, t), −9.30 to −9.19 (2F, t), −6.00 to −5.90 (2F, d), 6.35 to 6.41 (6F, q), 16.70 to 16.76 (6F, q). Mp 299 °C. Anal. Calcd for $C_{30}N_6OF_{17}B$: C, 45.37; H, 0; N, 10.58. Found: C, 45.12; H, 0; N, 11.19. HRMS (positive) exact mass calcd for $C_{30}N_6OF_{17}B$, 793.9955; found, 793.9968. Crystals of suitable quantity for X-ray diffraction were deposited as part of the train sublimation process.

Photoluminescence Quantum Efficiency. Solution photoluminescence quantum efficiencies (Φ_{PL}) were measured in spectroscopy grade toluene. The absorbance of each sample was measured to be >0.08 and their Φ_{PL} values were referenced to the previously reported value for **F_{12}BsubPc** of 0.4 (6b).

Photoelectron Spectroscopy Characterization. UPS measurements were performed using a PHI 5500 Multi-Technique system attached to a Kurt J. Lesker multiaccess chamber ultra high vacuum (UHV) cluster tool (base pressure of $\sim 1 \times 10^{-10}$). The spectrometer (hemispherical analyzer) was calibrated using XPS with monochromatic Al Kα ($h\nu$ = 1486.7 eV) as per ISO 15472 (17). The zero of the binding energy scale for all measurements was referenced to the Fermi level of a Ar^+ sputter-cleaned Au thin film (18) in electrical contact with the samples (i.e., on the same sample holder). The energy resolution for UPS measurements was ~135 meV determined from the width of the Fermi edge of Ar^+ sputter cleaned Au thin film (19). All UPS measurement were performed at a photoelectron takeoff angle of 90° and with a −15 V bias applied to the sample (20). The various organic molecules were deposited in a dedicated organic chamber from alumina crucibles [transfer arm evaporator (TAE) cell (21) onto freshly cleaved highly ordered pyrolytic graphite (HOPG) substrates. HOMO energy levels for each molecule were determined from 3 nm thick films as measured by a calibrated quartz crystal microbalance (QCM).

Materials for OLED Fabrication. Electronic grade copper phthalocyanine (CuPc) used as hole injection layer, *N*,*N*′-diphenyl-*N*,*N*′-bis-(1-naphthyl)-1-1′-biphenyl-4,4′-diamine (α-NPD) used as hole transport layer, and tris-(8-hydroxy-quinolinato)aluminum (Alq_3) used as emissive layer were provided by Norel Optronics Inc. and used as received. 1,3,5-Tris(*N*-phenylbenzimidazole-2-yl)benzene (TPBi) used as electron injection layer was purchased from Luminescence Technology Corp. and used as received. High-purity (99.99% trace metals basis) LiF and MoO_3 were purchased from Sigma-Aldrich and were thoroughly degassed in high vacuum prior to use.

OLED Fabrication and Characterization. OLEDs were fabricated in a Kurt J Lesker LUMINOS cluster tool (base pressure of $\sim 1 \times 10^{-8}$ Torr) using stainless steel shadow masks to define the device structure. Commercially patterned indium tin oxide (ITO) coated glass (50 mm × 50 mm) with a sheet resistance less than 15 Ω/□ was used for all devices in this study. Substrates were ultrasonically cleaned with a standard regiment of Alconox, acetone, and methanol followed by UV ozone treatment for 15 min. The various organic molecules were deposited from alumina crucibles (Knudsen cells) in a dedicated organic chamber. LiF was also deposited in the same chamber from alumina crucible. The Al cathode lines (2 mm wide) were deposited orthogonally to the ITO anode lines (1 mm wide) from a pyrolytic boron nitride crucible, in a separate metallization chamber without breaking vacuum. Film thicknesses were monitored using a calibrated QCM. The intersection of each cathode and anode line yields one OLED pixel, with 32 devices per substrate. The active area for all devices was 2 mm^2. A total of up to eight different device structures were fabricated on a single substrate to eliminate possible run-to-run variability caused by subtle variations in process conditions. Current−voltage (*IV*) characteristics of the OLEDs were measured using an HP4140B pA meter in ambient air. *IV* characteristics of the single carrier devices were measured in a vacuum cryostat (22) at 1×10^{-6} Torr. Luminance measurements were taken using a Minolta LS-110 Luminance meter. Electroluminescence (EL) spectra were measured using an Ocean Optics USB2000 fiber spectrometer.

RESULTS AND DISCUSSION

A. Synthesis of F_5subPcs, F_{12}subPc, and F_{17}subPc.

For our study, reliable supplies of both Cl-**BsubPc** (12) and Br-**F_{12}BsubPc** (13) were required, as they served as precursors to our synthetic targets. Because no reliable commercial sources could be identified we synthesized each in our laboratories by adapting their respective previously reported methods. The synthesis of Cl-**BsubPc** proceeds well as per the method of Kennedy; however, we found that a simple Soxhelt extraction with methanol was sufficient to purify to product past 99% (HPLC). In contrast, our attempts to reproduce the reported procedure for the synthesis of Br-**F_{12}BsubPc** generated a large quantity of byproducts and following the reported purification method (alumina column chromatograph) resulted in low yields. Because of the residual color left on the column, one can speculate that the Br-**F_{12}BsubPc** was irreversibly bound to the alumina through its reactive B−Br bond. After exploring several variations on normal column chromatography, we settled on the use of Kauffman column chromatography to purify crude Br-

F_{12}BsubPc (23). With this apparatus, continuously recycled hot solvent percolates through a packed chromatography bed thereby allowing for chromatography to be performed on compounds with limited solubility in the eluting solvent. However, this technique does require the selection of conditions which only the desired compound elutes and the impurities are irreversibly bound to the absorbent. Using this method, we successfully removed all but one impurity, using silica as the absorbent and dichloromethane as the eluting solvent. The major impurity could be isolated by stirring a portion of the post-Kauffman column mass in water for 12 h and filtering the insoluble solids (we do not make any claims that this process did not also harm the Br-**F_{12}BsubPc**). Single crystals suitable for X-ray crystallography and spectroscopic analysis were grown by simple evaporation of the water. Each characterization method employed identified the impurity as tetrafluorophthalimide including the X-ray diffraction of a single crystal. Using the combination of the reported synthetic conditions and Kaufmann column purification typically resulted in the post-Kaufmann column mass containing 20−30% of tetrafluorophthalmide (seen over 3 runs). Not convinced that washing with water would leave the Br-**F_{12}BsubPc** unaltered, we optimize the reaction conditions to minimize the formation of tetrafluorophthalimde using an experimental design. The procedure outlined in the Experimental Section represents the optimized conditions which produced the minimal amount of tetrafluorophthalimide (4% by HPLC analysis) after Kaufmann column purification. We have elected to use this material without further purification for the subsequent synthetic steps. The presence of small amounts of tetrafluorophthalimide does not interfere with the phenol substitution and we have found it is ultimately removed during the final purification by train sublimation.

The subsequent phenoxylation of Cl-**BsubPc** and Br-**F_{12}BsubPc** was carried out with 5 molar equiv. of the corresponding phenol by refluxing in either toluene or 1,2-dichlorobenzene. The conversion can easily be monitored using HPLC and/or TLC. Consistent with the method of Torres (4), we have found that the presence of 5 mol equiv. is necessary to achieve complete conversion of both Cl-**BsubPc** and Br-**F_{12}BsubPc** to their phenoxy derivatives regardless of reaction time. During our exploratory synthesis, we noted a significant difference in reactivity between Cl-**BsubPc** and Br-**F_{12}BsubPc** and the reacting phenol. The reaction of Cl-**BsubPc** with pentafluorophenol in refluxing toluene required 16 h for complete conversion, which was three times faster than for the reaction with Br-**F_{12}BsubPc** under identical conditions. To achieve complete conversions in a reasonable amount of time, we used 1,2-dichlorobenzene at reflux in place of toluene for the synthesis of **F_{12}BsubPc**, resulting in complete conversion in 20 h.

Material purity is essential to device performance in OLED devices; thus each phenoxy-**BsubPc** was rigorously purified prior to introduction into the UHV system and device fabrication. After synthesis, each of **F_5BsubPc**, **F_{12}BsubPc**, and **F_{17}BsubPc** was purified Kauffman column chromatography using silica as the absorbent and dichloromethane as the eluting solvent. **F_{17}BsubPc** required an additional purification by flash chromatography prior to sublimation on silica gel using dichloromethane as the eluent to remove some unidentified yet colored impurities. Finally each of **F_5BsubPc**, **F_{12}BsubPc**, and **F_{17}BsubPc** were purified by train sublimation (24).

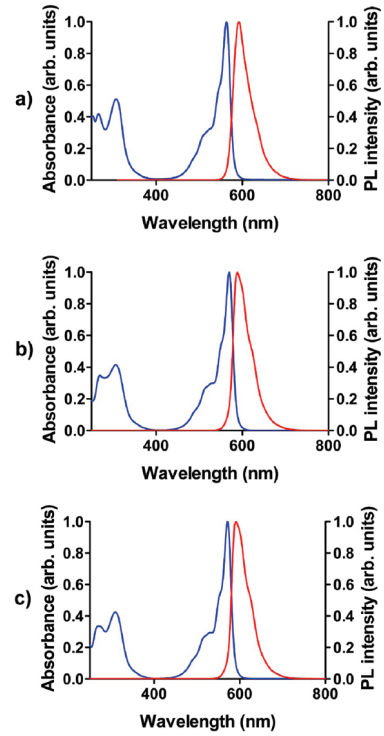

FIGURE 2. Absorption (blue) and photoluminescence (red) of (a) F_5subPc, (b) F_{12}subPc (middle), (c) F_{17}subPc in CH_2Cl_2.

B. Spectroscopy Analysis. The normalized UV−vis absorption spectra in dichloromethane for the each of **F_5BsubPc**, **F_{12}BsubPc**, and **F_{17}BsubPc** are shown in Figure 2 plotted alongside their respective photoluminescence spectra. Each derivative shares a similar absorption curve that is characteristic of **BsubPc** derivatives in general. The main absorption bands for **F_5BsubPc**, **F_{12}BsubPc**, and **F_{17}BsubPc** occur at λ_{max} 563, 569, and 571 nm with distinct shoulders at 547, 553, and 555 nm respectively. Fluorination shifts the absorption by approximately 6−8 nm toward the red (**F_5BsubPc** [$\lambda_{max} = 563$ nm] and **F_{12}BsubPc** [$\lambda_{max} = 569$ nm], **F_{17}BubPc** [$\lambda_{max} = 571$ nm]).

The photoluminescence (PL) of each compound was measured by excitation at the λ_{max} in dichloromethane solution (Figure 2). The PL spectrum of **F_5BsubPc** shows a peak emission at 592 nm corresponding to a Stokes shift of 29 nm with significant red tailing as the mirror image of its absorption shoulder. Both **F_{12}BsubPc** and **F_{17}BsubPc** showed a shorter Stokes shift of 20 nm, each having an emission at 589 and 591 nm with well-defined shoulders at 617 and 620 nm (respectively) reflecting their absorption spectra.

The solid -state UV−vis absorption spectra were also measured for each of **F_5BsubPc**, **F_{12}BsubPc**, and **F_{17}BsubPc** from their thin films formed by sublimation onto a quartz substrate. These films each exhibited a shift in their absorp-

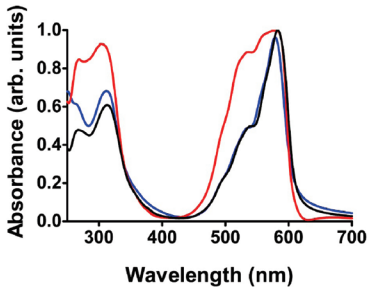

FIGURE 3. Solid-state UV−vis absorption spectra of F_5BsubPc (blue), F_{12}subPc (red), and F_{17}BsubPc (black) on quartz.

tion spectrum from their solution absorption spectra, with a shift in λ_{max} for **F_5BsubPc** of 16 nm [λ_{max} = 579 nm], for **F_{12}BsubPc** of 12 nm [λ_{max} = 581 nm], and for **F_{17}BsubPc** of 12 nm [λ_{max} = 583 nm] (Figure 3). We also observed that the absorption spectrum of **F_{12}BsubPc** was significantly broadened compared to its solution spectrum, whereas the solid state absorption spectrum of **F_5BsubPc** and **F_{17}BsubPc** did not exhibit significant broadening.

Room-temperature photoluminescent quantum yields (Φ_{PL}) were measured for **F_5BsubPc** and **F_{17}BsubPc** using the previously reported quantum yield for **F_{12}BsubPc** of 0.40 (6b) as a reference. The measurements were performed in purged toluene on dilute solutions, each with an absorbance below 0.08. We observed similar quantum yields for each of the three compounds, although a slight decrease with increasing fluorination was observed from **F_5BsubPc** [Φ_{PL} = 0.42] to **F_{12}BsubPc** [Φ_{PL} = 0.40] and **F_{17}BsubPc** [Φ_{PL} = 0.38], respectively.

C. Crystal Structure Analysis. As we targeted each of **F_5BsubPc**, **F_{12}BsubPc**, and **F_{17}BsubPc** for use as thin solid films in OLEDs it is of interest to examine how each arranges itself within the solid state. For this purpose, we successfully grew single crystals suitable for X-ray diffraction for each compound. Single crystals of **F_5BsubPc** and **F_{12}BsubPc** were formed by slow vapor diffusion crystallization of heptane (poor solvent) into benzene (good solvent). Our attempts to grow single crystals of **F_{17}BsubPc** using the same method did not produce crystals of suitable quality for diffraction however, high-quality single crystals were formed during train sublimation.

If you consider the shape and structural features of the native **BsubPc** (Figure 1), the interaction of adjacent **BsubPc** molecules within a crystal lattice could be described first by the interaction of the bowl-shaped faces of each **BsubPc** (concave−concave, convex−convex, or concave−convex), and second by considering the interdigitated arrangement of the **BsubPc**s isoindoline units through space and by calling one side of the **BsubPc** ligand the "tail" and the other the "head" (Figure 4). As of the date of this submission, the Cambridge Crystallographic Database (CCD) contains seventeen crystal structures of eleven chemically different **BsubPc** compounds (Table 1) (10, 25). Nine of the eleven chemically different structures are of hydrogenated **BsubPc**s, which tend to associate in one of three modes: the predominant mode is a concave−concave head-to-head arrangement followed by a convex−convex head-to-head and then

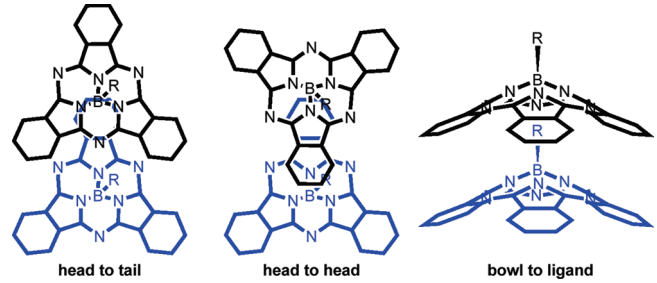

FIGURE 4. Common arrangements for intermolecular association of BsubPc (double bonds omitted for clarity).

Table 1. Bonding Arrangement Count in the CCD of BsubPc−BsubPc Interactions

BsubPc	concave−concave head-to-head	concave−concave head-to-tail	convex−convex head-to-head	concave-to-ligand
CCD	7	2	5	2
F−F_{12}BsubPc				1
F_5BsubPc	1			
F_{12}BsubPc				1
F_{17}BsubPc				1

a concave−concave head-to-tail arrangement (Figure 5). Recently, we have developed a compound with a convex tail-to-tail association demonstrating that these three modes of association can be expanded upon (16). The remaining two examples in the CCD are fluorinated **BsubPcs** Cl-**F_{12}BsubPc** and phenoxy-**F_{12}BsubPc**. These two structures and one additional report unpublished in the CCD of F-**F_{12}BsubPc** represent all of the crystallographic data on fluorinated **BsubPcs**. Each has a similar arrange in the solid state that is uniquely different from their nonfluorinated counterparts: they arrange in a concave-to-axial ligand motif, whereby the axial ligand of one **BsubPc** resides in the space of the concaved side of another (the bowl of a neighboring **BsubPc**, Figure 4).

The crystal structure of **F_5BsubPc** exemplifies the predominant arrangement of **BsubPcs**: each **F_5BsubPc** is aligned with a neighboring **F_5BsubPc** in a concave−concave head-to-head fashion, which directs the formation of intermolecular dimers shown in structures a and d in Figure 5. In **F_5BsubPc**, the peripheral six-membered ring of the isoindoline subunit (blue) overlaps with the five-membered ring of the isoindoline subunit of its neighboring **BsubPc** (red) with a ring centroid proximity of 3.518 Å. In this arrangement, the boron centers of the dimer pairs are separated by 8.464 Å. Each **F_5BsubPc** pair is separated by 11.140 Å in the *a* axis, 10.364 Å along the *b* axis, and 12.410 Å in the *c* axis.

The crystal structure we obtained for **F_{12}BsubPc** is an example of aforementioned concaved-to-ligand association and is identical to the previously reported structure despite being grown under different conditions (10). In its structure, the strongest interaction occurs between the axial phenoxy group and one of the **BsubPc** isoindoline units (Figures 5b,e). The ring centroid proximity from the phenoxy group (green) to the five-membered ring of the isoindoline subunit (red) is closest at 3.605 Å, whereas the distance to the six-membered ring (blue) is 3.726 Å. The **F_{12}BsubPc** pairs are

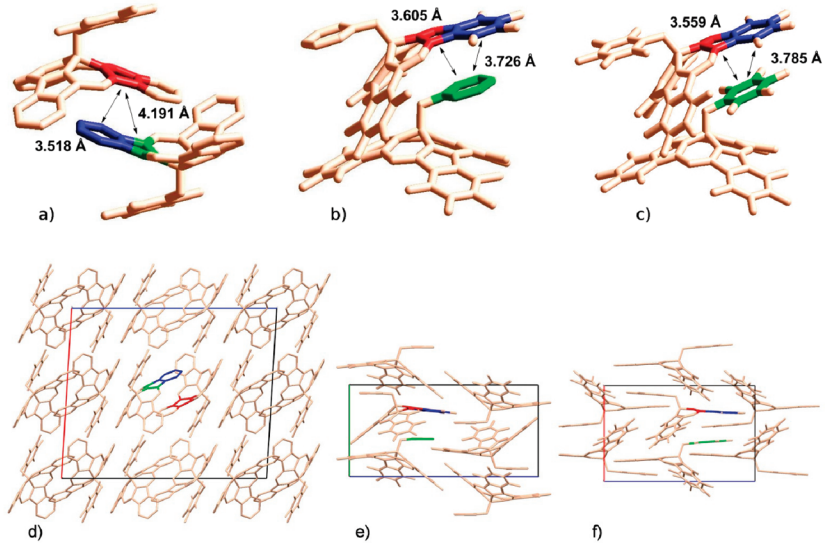

FIGURE 5. Crystal arrangement of two neighboring BsubPc derivatives [(a) F_5subPc, (b) F_{12}subPc, and (c) F_{17}BsubPc] with intermolecular distances highlighted, followed by the unit cells for (d) F_5subPc, (e) F_{12}subPc, and (f) F_{17}BsubPc.

Table 2. Photophysical and Electronic Properties of F_5BsubPc, F_{12}BsubPc, and F_{17}BsubPc

	$\lambda_{max,abs}$ (nm)[c]	$\lambda_{max,abs}$ (nm) thin film	$\lambda_{max,PL}$ (nm)[c]	$\lambda_{max,EL}$ (nm)	$E_{g,opt}$ (eV)	E^1_{red} (mV)[c]	E^1_{red} (mV)[d]	LUMO (eV)	HOMO (eV)	Φ_{PL} (%)
Cl-**BsubPc**	565	590			2.0			3.6 (a)	5.6 (8)	
					1.9			3.8 (b)	5.7 (9a)	
F_5BsubPc	563	579	592	601	2.1	−878[a]	−860[b]	3.76	5.86	0.42
						−889[b]				
F_{12}BsubPc	569	581	589	601	2.1	−571[b]	−522[b]	4.51	6.61	0.40(6b)
F_{17}BsubPc	571	583	591	601	2.1	−523[b]	−493[b]	4.55	6.65	0.38
C_{60}								4.1	6.4	

[a] Measured half-wave potential. [b] Peak potential. [c] In CH_2Cl_2. [d] In CH_3CN.

Table 3. Material pProperties of F_5BsubPc, F_{12}BsubPc, and F_{17}BsubPc; Sublimation Temperature Measured at ~1 × 10^{-10} Torr in UHV Apparatus

	melting point (°C)	sublimation temperature (°C)
F_5BsubPc	280	180
F_{12}BsubPc	342	180
F_{17}BsubPc	299	160

separated by 11.540 Å in the *a* axis, 5.338 Å along the *b* axis, and 11.009 Å in the *c* axis.

A similar concaved-to-ligand association occurs in the crystal structure of **F_{17}BsubPc**. Once again, the strongest association occurs between the axial pentafluorophenoxy and one of the indoline units from the nieghbouring **BsubPc** (Figure 5c,f). The **F_{17}BsubPc** are separated by 5.425 Å in the *a* axis, 15.075 Å along the *b* axis, and 11.131 Å in the *c* axis.

D. Sublimation and Melting Point. We have synthesized these fluorinated phenoxy-**BsubPc** derivatives to generate **BsubPc**s with low sublimation points (s.p.) due to the nonassociative nature of organic fluorine. Prior to synthesis, we hypothesized that as the degree of fluorination was increased their melting point (m.p.) and s.p. would decrease. Contrary to our initial hypothesis, the melting point (m.p.) and s.p. of the **BsubPc**s were not arranged in this order (Table 3). Although these results are nonintuitive, their differences can be explained by their differences in crystal structure. **F_{12}BsubPc** and **F_{17}BsubPc** possess similar columnar crystal packing; thus between these two compounds, **F_{17}BsubPc** should have a lower melting point (m.p.) and s.p., as observed. **F_5BsubPc** packs in markedly different dimer arrangement whereby no long-range aromatic overlap propagates through its structure, thereby deviating it from the hypothesized trend. Rather, **F_5BsubPc** had the lowest melting point (m.p.) at 280 °C and a s.p. identical to that of **F_{12}BsubPc** at 180 °C.

E. Cyclic Voltammetry. Solution cyclic voltammetry (CV) of the **F_5BsubPc**, **F_{12}BsubPc**, and **F_{17}BsubPc** was performed in order to allow us to classify both the nature of their electrical activity (*n*-type or *p*-type) and the position of their LUMO and HOMO. We performed CV measurements in both dichloromethane (DCM) and acetonitrile (ACN) with tetrabutylammonium perchlorate (Bu_4NClO_4) as the electrolyte and all potentials were corrected to decamethylferrocene (present as an internal standard). The half-wave reduction potential ($E_{1/2,red}$) of decamethylferrocene was previously measured to be −0.012 V vs Ag/AgCl (15).

We initially scanned all samples over the range +1.6 to −1.6 V in both DCM and ACN. What we observed was that neither **F_{12}BsubPc** or **F_{17}BsubPc** underwent an oxidation event in either solvent—they did not form radical cations (current measured to 10 μA). Rather, we observed that **F_{12}BsubPc** and **F_{17}BsubPc** exhibited only *n*-type behavior; that is, they formed only radical anions. Although **F_5BsubPc**

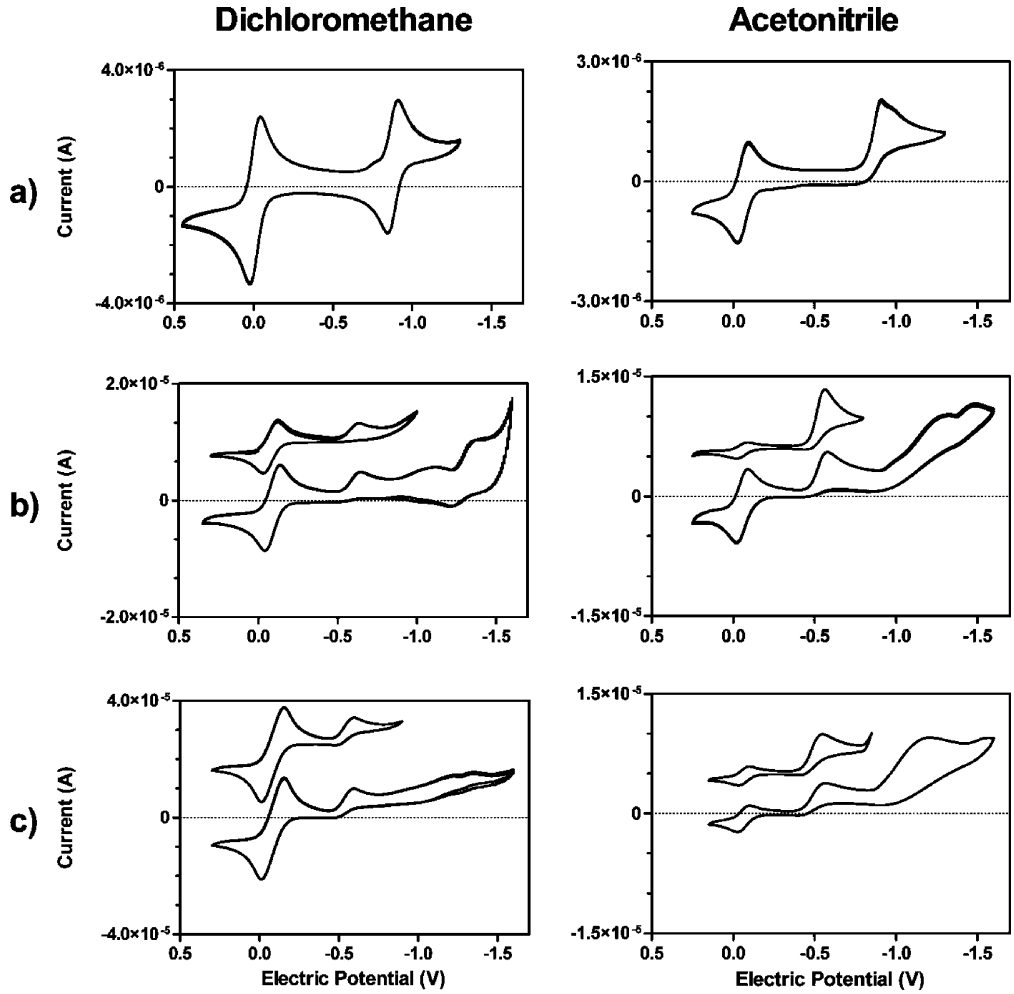

FIGURE 6. Cyclic voltammograms of (a) F_5BsubPc, (b) F_{12}BsubPc, and (c) F_{17}BsubPc in both dichloromethane and acetonitrile with 0.1 M Bu_4NClO_4 as supporting electrolyte at room temperature (22.5 °C) and a scanning rate of 100 mV/s.

did undergo an irreversible oxidation at +1.155 V and exhibited a reversible reduction peak having a half-wave potential ($E^1_{1/2,red}$) of −878 mV in DCM solution (Figure 6a, Table 2). Interestingly, in ACN the reduction of **F_5BsubPc** to its radical anion was not reversible but we did measure the peak potential ($E^1_{p,red}$) to be −860 mV. For comparison, the peak reduction potential in DCM is −889 mV. In the case of **F_5BsubPc**, no evidence was found that radical anion underwent an additional reduction. In the case of **F_{12}BsubPc** and **F_{17}BsubPc**, no reversible reduction could be observed (Figure 6b,c) although each underwent an irreversible reduction. **F_{12}BsubPc** shows an irreversible reduction with a peak potential of −571 mV in DCM and −522 mV in ACN. **F_{17}BsubPc** possess less negative peak potential at −523 mV in DCM and −493 mV in ACN. When we scan **F_{12}BsubPc** and **F_{17}BsubPc** to higher negative potential, we see evidence of multiple reduction events, albeit all are irreversible. Our results were repeated and are consistent in our laboratory but are in contradiction to previous reports of the cyclic voltammetry of **F_{12}BsubPc**, which found the reduction to occur reversibly; however, a different working electrode, electrolyte, and solvent were used (6b).

The presence of fluorine in place of hydrogen in both the peripheral (around the **BsubPc** chromaphore) and axial (on the phenoxy ring) positions strongly affects the reduction potential of these compounds. Axial fluorination (averaged between both solvents) decreased $E^1_{p,red}$ by 37 mV on going from **F_{12}BsubPc** and **F_{17}BsubPc**. Whereas peripheral fluorination decreased the $E^1_{p,red}$ by 362 mV on going from **F_5BsubPc** to **F_{12}BsubPc**.

F. Photoelectron Spectroscopy. Ultraviolet photoelectron spectroscopy (UPS) was used to measure the absolute HOMO energy-levels of **F_5BsubPc**, **F_{12}BsubPc**, and **F_{17}BsubPc** in the solid state. Figure 7 shows the He $I\alpha$ ($h\nu$ = 21.22 eV) valence band spectra and secondary electron cutoff of the molecules deposited on freshly cleaved HOPG. HOPG substrates were chosen to minimize final-state hole-screening effects, which can introduce significant artifacts into energy-level measurements. In the valence band spectra shown in Figure 7b, the peak at low binding energy (for each molecule) is derived from the density of states (DOS) corresponding to the HOMO. Analogous to a Schottky contact at a metal/semiconductor interface, a barrier height for hole injection (ϕ_{B_p}) is typically defined as the offset between the Fermi level of the substrate (0 eV binding energy) and the onset of the HOMO derived peak. The energetic position of the HOMO derived peak (i.e., the value of ϕ_{B_p}) for **F_5BsubPc**,

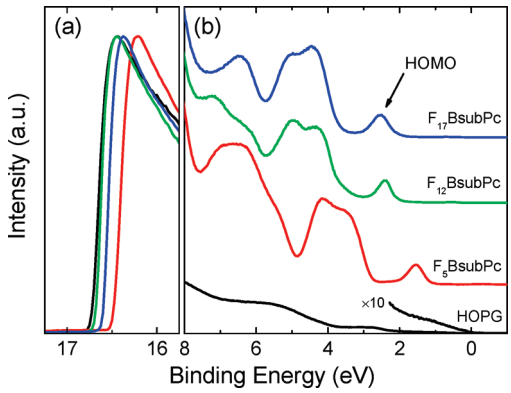

FIGURE 7. UPS He *I*α (hν = 21.22 eV) valence band spectra of F_5BsubPc, F_{12}BsubPc,and F_{17}BsubPc deposited on HOPG showing (a) the secondary electron cutoff, and (b) the HOMO-derived peak of the molecules.

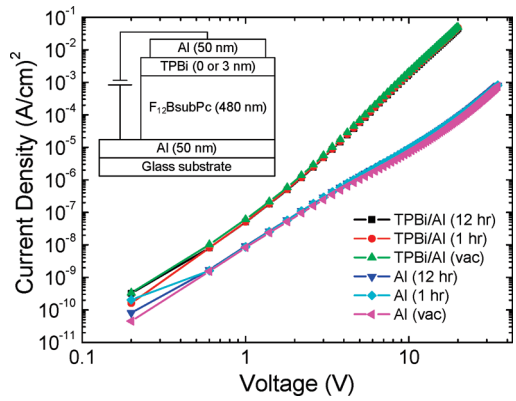

FIGURE 8. Current density as a function of voltage for F_{12}BsubPc single carrier devices with and without TPBi electron injection layers. *IV* characteristics measured in vacuum and after air exposure for 1 and 12 h are shown for both structures. The device structure is shown in the inset.

F_{12}BsubPc, and **F_{17}BsubPc** is determined by both the HOMO energy level as well as the interfacial dipole at the HOPG/organic interface. The HOMO energy level (relative to vacuum) can be determined from ϕ_{B_p} as follows (26)

$$E_{\mathrm{HOMO}} = e(\phi_{B_p} + \phi_{\mathrm{m,eff}}) \quad (1)$$

where $\phi_{\mathrm{m,eff}}$ is the effective work function (27) of the organic overlayer. A detailed discussion of work function measurements using UPS can be found in ref 20.

The calculated HOMO energy levels of **F_5BsubPc**, **F_{12}BsubPc**, and **F_{17}BsubPc** using eq 1 are summarized in Table 1, along with the values measured for C_{60} as reference. The HOMO energy levels measured by UPS follow the same trend as the LUMOs measured by CV (i.e., the HOMO energy levels decrease with the degree of fluorination). However, although peripheral fluorination decreased the HOMO energy level by 0.77 eV, the LUMO energy level was reduced by only 0.36 eV. Because the optical gap is nearly identical for **F_5BsubPc**, **F_{12}BsubPc**, and **F_{17}BsubPc** (see Table 1), this discrepancy is most likely due to the different techniques used to measure the HOMO and LUMO (i.e., UPS in the solid state vs CV in solution) (28) rather than any significant change in the HOMO−LUMO gap. Additional experiments and theoretical calculations are underway to confirm this hypothesis, the results of which will be published elsewhere.

G. Single Carrier Devices. Air-stable carrier transport characteristics are highly desirable for improving the lifetime and stability of organic electronic devices. In particular, air-stable *n*-type materials are highly sought-after since most *n*-type organic semiconductors are oxidatively unstable. For example, the transport characteristics of C_{60} and C_{60} derivatives, such as [6,6]-phenyl-C_{61} butyric acid methyl ester (PCBM), degrade rapidly upon exposure to air (29). Fluorination of various organic semiconductors has been shown to effective yield materials with air-stable *n*-type conductivity (30). To demonstrate the air-stable *n*-type transport characteristics of the new **F_5BsubPc**, **F_{12}BsubPc**, and **F_{17}BsubPc** molecules, we fabricated single-carrier (22) electron-only devices with the structure: Al (50 nm)/organic (~500 nm)/Al (50 nm). Figure 8 shows the *IV* characteristics for **F_{12}BsubPc** single carrier devices measured in vacuum and after air exposure for 1 and 12 h. Even after several days air exposure, the *IV* characteristics were unchanged, indicating that **F_{12}BsubPc** is not only air-stable but may also help passivate the Al electrodes from oxidation. Similar results were found for **F_5BsubPc** and **F_{17}BsubPc**. In contrast, Al/C_{60}/Al single carrier devices were previously shown to degrade by nearly 3 orders of magnitude (in terms of current density at a given voltage) after only 1 h exposure to air (31).

Figure 7 also shows the *IV* characteristics for **F_{12}BsubPc** single carrier devices with a 3 nm thick 1,3,5-tris(*N*-phenylbenzimidazole-2-yl)benzene (TPBi) electron-injection layer inserted between the organic layer and the top Al cathode (i.e., Al/ **F_{12}BsubPc**/TPBi/Al). Remarkably, the thin TPBi injection layer increased the injection current density by nearly 3 orders of magnitude, indicating a significant reduction in the injection barrier height for electrons at the **F_{12}BsubPc**/Al interface (32). Similar results were found for **F_5BsubPc** and **F_{17}BsubPc**. We also tested several other common cathode structures (e.g., LiF/Al), but found that TPBi/Al yielded the best results.

The improvement in electron injection with TPBi interlayer is quite unexpected given the low lying LUMOs (see Table 2) of the three molecules. The Al cathode, with a low work function of ~4.2 eV should easily be able to inject electrons into any of the three molecules. The poor electron injection for the bare Al cathode suggests one of two possibilities: (i) either the organic is degraded by the hot Al atoms condensing from the vapor phase, similar to the case of Alq_3/Al (33), or (ii) the Fermi level of the cathode is pinned by the organic. Given that the reverse bias current (i.e., electron injection from the bottle Al anode) is equally as poor as the forward bias current, Fermi level pinning is the most likely culprit. A similar effect has been experimentally observed for other strong electron acceptors such as C_{60} (34).

H. Organic Light-Emitting Diodes. To demonstrate the EL characteristics of the new **F_5BsubPc**, **F_{12}BsubPc**, and **F_{17}BsubPc** molecules, we fabricated single-layer OLEDs with the structure: ITO/**BsubPc** (~45 nm)/TPBi (3 nm)/Al (100 nm). For the **F_{12}BsubPc** and **F_{17}BsubPc**, an additional

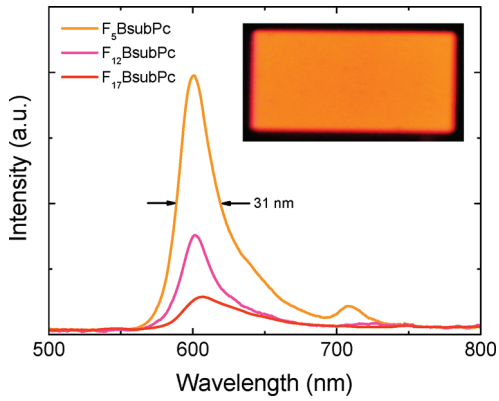

FIGURE 9. EL spectra of OLED devices with F_5BsubPc, F_{12}BsubPc, and F_{17}BsubPc emissive layers. The inset shows an optical micrograph of an illuminated OLED with F_5BsubPc emissive layer. The area of the illuminated OLED is 1 mm × 2 mm.

hole-injection layer of MoO_3 (1 nm) was required at the anode contact (i.e., ITO/MoO_3/**BsubPc**) to facilitate hole injection into the deeper HOMO levels. Although weak EL emission was observed for all three molecules, the driving voltage (for a given luminance of 1 cd/m^2) was greater than 15 V. Because good electron injection and transport is expected on the basis of the single carrier device results (35), the single-layer OLEDs are most likely hole deficient. In such a case, the emission zone is typically localized near the anode, resulting in significant exciton quenching (36).

To improve the injection of holes and prevent exciton quenching to the anode, we fabricated trilayer OLEDs with the structure: ITO/CuPc (25 nm)/α-NPD (45 nm)/**BsubPc** (~45 nm)/TPBi (3 nm)/Al (100 nm). Both the turn-on voltage and luminance were significantly improved over the single-layer devices. For example, for **F_5BsubPc** the turn-on voltage was reduced to 3.4 V, which is comparable to the value of 3.2 V for a standard Alq_3 green OLED (37). However, despite a similar driving voltage to the standard Alq_3 green OLED, the luminance is still quite low. The maximum luminance of the **F_5BsubPc** trilayer OLED was 122 cd/m^2 at 8 V, with a maximum current efficiency of 0.03 cd/A, which is several orders of magnitude lower than the typical ~4 cd/A for a standard Alq_3 trilayer OLED (see Figure S7 in the Supporting Information). From the luminous efficacy and EL spectra (see Figure 9), the calculated external quantum efficiency (EQE) of the **F_5BsubPc** trilayer OLED is 0.013%. Assuming an optical outcoupling factor of 20%, this implies an internal quantum efficiency (IQE) of only 0.065%, much less than the PL quantum efficiency measured in solution (42%). The disparity between the electroluminescence for **F_5BsubPc** and its Φ_{PL} suggest that there is significant room for improved performance of **F_5BsubPc** through device optimization (including materials selection). The maximum luminance of the **F_{12}BsubPc** and **F_{17}BsubPc** devices was significantly lower than that of **F_5BsubPc**, with a maximum value of <1 cd/m^2. The poor performance of these devices could be attributed to the large hole injection barrier at the α-NPD/**BsubPc** interface because of the much deeper HOMO of **F_{12}BsubPc** and **F_{17}BsubPc** (~6.6 eV). Again, it might be possible to dramatically improve this performance through device optimization.

Figure 9 shows the measured EL spectra of the trilayer OLEDs; similar results were obtained for the single-layer devices, albeit with much weaker intensities. The EL emission for the three molecules is nearly identical with a peak maximum at 601 nm. Interestingly, a small subpeak was observed in the **F_5BsubPc** EL spectra, which was not observed in the solution-phase fluorescence spectra. However, a weak high-wavelength absorption peak was observed in the thin film UV−vis spectra (see Figure 3) which may be the source of this weak high-wavelength emission. Although a similar feature was observed in the thin film UV−vis spectra of **F_{12}BsubPc** and **F_{17}BsubPc**, no corresponding peak was observed in the EL because of the noise limit of the detector.

Recently, Díaz et al. (7) reported that **BsubPc** derivatives exhibit spectrally narrow EL emission. The full width at half-maximum (fwhm) of our EL spectra are remarkably narrow at only ~30 nm, which is significantly better than the ~60 nm fwhm reported by Díaz et al. (7). Their device architecture utilized **BsubPc** as a fluorescent dopant in a blue-emitting polymeric host. Such device architecture relies on the host polymer for charge transport and exciton formation. Energy is subsequently transferred from the host excited state to the **BsubPc** dopant through a Förster-type energy-transfer process. However, in our device architectures, electrons and holes are injected into the **BsubPc** emissive later, resulting in direct exciton formation on the **BsubPc** derivative. As of yet, it is unclear if the superior bandwidth of our devices is due to the device architecture or rather a result of the molecular structure differences.

CONCLUSION

A series of fluorinated phenoxy-**BsubPc** compounds have been synthesized in high yield and rigorously purified using both Kauffman column and train sublimation techniques. They have been characterized by single-crystal XRD along with ^{1}H NMR and ^{19}F NMR analysis. The crystal packing of **F_5BsubPc** revealed a distinct concave−concave head-to-head association common to hydrogenated **BsubPc**s, whereas **F_{12}BsubPc** and **F_{17}BsubPc** packed in a concave-to-ligand fashion, predominant in fluorinated **BsubPc**s. It is probable that their differences in crystal packing has affected their melting and sublimation points. UV−vis λ_{max} of each of these compounds increased in relation to the degree and location of fluorination, such that λ_{max} **F_5BsubPc** < **F_{12}BsubPc** < **F_{17}BsubPc** in both the solid and liquid state. Each of these compounds fluoresced strongly between a narrow range from 589 to 592 nm. The fluorescence stokes shift for **F_5BsubPc** was 29 nm, whereas both the peripherally fluorinated **F_{12}BsubPc** and **F_{17}BsubPc** were shifted by 20 nm. Photoluminescent quantum yields for **F_5BsubPc** and **F_{17}BsubPc** decreased with increasing fluorination from 0.42 to 0.38, respectively. The cyclic voltammagrams of **F_{12}BsubPc** and **F_{17}BsubPc** compounds showed no oxidative behavior. On the reductive side, only **F_5BsuBPc** showed reversibility in dichloromethane but in acetonitrile it reduced

irreversibly, whereas both **F_{12}BsubPc** and **F_{17}BsubPc** had irreversible reduction peaks in each solvent. Peripheral fluorination of **BsubPc** shifted the reductive peak by −362 mV, whereas axial fluorination shifted the reductive peak by −37 mV. All three compounds demonstrated air stable *n*-type conductivity in single carrier devices. Orange-colored EL emission was observed from single-layer, vacuum-deposited OLEDs for the first time. Trilayer OLEDs with the three molecules severing as emission layer yielded significantly improved results with extremely narrow EL emission with a fwhm of only ∼30 nm; In particular, **F_5BsubPc** showed a maximum luminescence of 122 cd/m^2 at 8 V, with a maximum current efficiency of 0.03 cd/A. Although the results for this initial device containing **F_5BsubPc** as an emitter were rather low, the disparity between the maximum current efficiency and the Φ_{PL} demonstrates that there is substantial room for improvement and we are currently working to optimize an OLED structure based on **F_5BsubPc**.

Acknowledgment. We acknowledge funding for this research from Natural Sciences and Engineering Research Council (NSERC) of Canada. The authors also acknowledge the contributions of Mr. Jack O'Donnell (glassblower, Chemistry Department at the University of Toronto).

Supporting Information Available: Crystallographic information (CIF); full description of the Kauffman column and the train sublimation apparatus and device performance comparison between **F_5BsubPc** and Alq_3 (PDF). This material is available free of charge via the Internet at http://pubs.acs.org.

REFERENCES AND NOTES

(1) Meller, A.; Ossko, A. *Monatsh. Chem.* **1972**, *103*, 150–155.

(2) (a) Kobayashi, N.; Kondo, R.; Nakajima, S.; Osa, T. *J. Am. Chem. Soc.* **1990**, *112* (26), 9640–9641. (b) Kobayashi, N.; Ishizaki, T.; Ishii, K.; Konami, H. *J. Am. Chem. Soc.* **1999**, *121* (39), 9096–9110.

(3) Torres, T. *Angew. Chem., Int. Ed.* **2006**, *45*, 2834–2837.

(4) Claessens, C. G.; Gonzalez-Rodriguez, D.; del Rey, B.; Torres, T.; Mark, G.; Schuchmann, H. P.; von Sonntag, C.; MacDonald, J. G.; Nohr, R. S. G. *Eur. J. Org. Chem.* **2003**, *14*, 2547–2551.

(5) Claessens, C. G.; Gonzalez-Rodriguez, D.; McCallum, C. M.; Nohr, R. S.; Schuchmann, H. P.; Torres, T. *J. Porphyrins Phthalocyanines* **2007**, *11* (3−4), 181–188.

(6) (a) Gonzalez-Rodriguez, D.; Torres, T.; Olmstead, M. M.; Rivera, J.; Herranz, M. A.; Echegoyen, L.; Castellanos, C. A.; Guldi, D. M. *J. Am. Chem. Soc.* **2006**, *128*, 10680–10681. (b) Gonzalez-Rodriguez, D.; Torres, T.; Guldi, D. M.; Rivera, J.; Herranz, M. A. A.; Echegoyen, L. *J. Am. Chem. Soc.* **2004**, *126*, 6301–6313.

(7) Díaz, D. D.; Bolink, H. J.; Cappelli, L.; Claessens, C. G.; Coronado, E.; Torres, T. *Tetrahedron Lett.* **2007**, *48*, 4657–4660.

(8) Chen, Y.-H.; Chang, J.-H.; Lee, G.-R.; Wu, I.-W.; Fang, J.-H.; Wu, C.-I. *Appl. Phys. Lett.* **2009**, *95*, 133302.

(9) (a) Mutolo, K. L.; Mayo, E. I.; Rand, B. P.; Forrest, S. R.; Thompson, M. E. *J. Am. Chem. Soc.* **2006**, *128*, 8108–8109. (b) Gommans, H.; Cheyns, D.; Aernouts, T.; Girotto, C.; Poortmans, J.; Heremans, P. *Adv. Funct. Mater.* **2007**, *17*, 2653–2658. (c) Gommans, H.; Aernouts, T.; Verreet, B.; Heremans, P.; Medina, A.; Claessens, C. G.; Torres, T. *Adv. Funct. Mater.* **2009**, *19*, 3435–3439. (d) Kumar, H.; Kumar, P.; Bhardwaj, R.; Sharma, G. D.; Chand, S.; Jain, S. C.; Kumar, V. *J. Phys. D: Appl. Phys.* **2009**, *42*, 015103. (e) Ma, B.; Woo, C. H.; Miyamoto, Y.; Frechet, J. M. J. *Chem. Mater.* **2009**, *21*, 1413–1417. (f) Klaus, D.; Knecht, R.; Dragässer, A.; Keil, C.; Schlettwein, D. *Phys. Status Solidi A* **2009**, *206* (12), 2723–2730. (g) Ma, B.; Miyamoto, Y.; Woo, C. H.; Fréchet, J. M. J.; Zhang, F.; Liu, Y. *Proc. SPIE* **2009**, *7416*, 74161E-1.

(10) Claessens, C. G.; Torres, T. *Angew. Chem., Int. Ed.* **2002**, *41* (14), 2561–2565.

(11) Milian Medina, B.; Beljonne, D.; Egelhaaf, H. J.; Gierschner, J. *J. Chem. Phys.* **2007**, *126*, 111101.

(12) Zyskowski, C. D.; Kennedy, V. O. *J. Porphyrins Phthalocyanines* **2000**, *4*, 707–712.

(13) Sharman, W. M.; van Lier, J. E. *Bioconjugate Chem.* **2005**, *16* (5), 1166–1175.

(14) Spek, A. L. *J. Appl. Crystallogr.* **2003**, *36*, 7–13.

(15) Bender, T. P.; Graham, J. F.; Duff, J. M. *Chem. Mater.* **2001**, *13*, 4105–4111.

(16) Morse, G. E.; Paton, A. S.; Lough, A.; Bender, T. P. *Dalton Trans.* **2010**; DOI: 10.1039/ b922199a.

(17) Seah, M. P. *Surf. Interface Anal.* **2001**, *31*, 721.

(18) Helander, M. G.; Greiner, M. T.; Wang, Z. B.; Lu, Z. H. *Appl. Surf. Sci.* **2009**, *255*, 9553.

(19) Tsai, K. Y. F.; Helander, M. G.; Lu, Z. H. *J. Appl. Phys.* **2009**, *105*, 083706.

(20) Helander, M. G.; Greiner, M. T.; Wang, Z. B.; Lu, Z. H. *Appl. Surf. Sci.* **2008**; doi:10.1016/j.apsusc.2009.11.002.

(21) Greiner, M. T.; Helander, M. G.; Wang, Z. B.; Lu, Z. B. *Rev. Sci. Instrum.* **2009**, *80*, 125101.

(22) Helander, M. G.; Wang, Z. B.; Greiner, M. T.; Qiu, J.; Lu, Z. H. *Rev. Sci. Instrum.* **2009**, *80*, 033901.

(23) Kauffman, J. M.; Bjorkman, C. O. *J. Chem. Educ.* **1976**, *53* (1), 33.

(24) Wagner, H. J.; Loutfy, R. O.; Hsiao, C. K. *J. Mater. Sci.* **1982**, *17* (10), 2781–2791.

(25) (a) Kietaibl, H. *Monatsh. Chem.* **1974**, *105*, 405–418. (b) Rauschnabel, J.; Hanack, M. *Tetrahedron Lett.* **1995**, *36* (10), 1629–1632. (c) Engel, M. K.; Yao, J.; Maki, H.; Takeuchi, H.; Yonehara, H.; Pac, C. *Kawamura Rikagaku Kenkyusho Hokoku* **1997**, 53–65; CA130:39766. (d) Potz, R.; Göldner, M.; Hückstädt, H.; Cornelissen, U.; Tutaβ, A.; Homborg, H. Z. *Anorg. Allg. Chem.* **2000**, *626*, 588–596. (e) Fukuda, T.; Stork, J. R.; Potucek, R. J.; Olmstead, M. M.; Noll, B. C.; Kobayashi, N.; Durfee, W. S. *Angew. Chem., Int. Ed.* **2002**, *41* (14), 2565–2568. (f) Fukuda, T.; Olmstead, M. M.; Durfee, W. S.; Kobayashi, N. *Chem. Commun.* **2003**, 1256–1257. (g) Kato, T.; Tham, F. S.; Boyd, P. D. W.; Reed, C. A. *Heteroat. Chem.* **2006**, *17* (3), 209–216.

(26) Ishii, H.; Hayashi, K.; Ito, E.; Seki, K. *Adv. Mater.* **1999**, *11*, 605.

(27) (a) Helander, M. G.; Wang, Z. B.; Qiu, J.; Lu, Z. H. *Appl. Phys. Lett.* **2008**, *93*, 193310. (b) Helander, M. G.; Wang, Z. B.; Greiner, M. T.; Qiu, J.; Lu, Z. H. *Appl. Phys. Lett.* **2009**, *95*, 083301.

(28) (a) D'Andrade, B. W.; Datta, S.; Forrest, S. R.; Djurovich, P.; Polikarpov, E.; Thompson, M. E. *Org. Electron.* **2005**, *6*, 11. (b) Djurovich, P.; Mayo, E. I.; Forrest, S. R.; Thompson, M. E. *Org. Electron.* **2008**, *10*, 515.

(29) (a) Dodabalapur, A.; Katz, H. E.; Torsi, L.; Haddon, R. C. *Science* **1995**, *269*, 1560. (b) Anthopoulos, T. D.; De Leeuw, D. M.; Cantatore, E.; Setayesh, S.; Meijer, E. J. *Appl. Phys. Lett.* **2004**, *85*, 4205.

(30) Ye, R.; Baba, M.; Mori, K. *Jpn. J. Appl. Phys.* **2005**, *44*, L581.

(31) Huang, C. J.; Grozea, D.; Turak, A.; Lu, Z. H. *Appl. Phys. Lett.* **2005**, *86*, 033107.

(32) Wang, Z. B.; Helander, M. G.; Tsang, S. W.; Lu, Z. H. *Phys. Rev. B* **2008**, *78*, 193303.

(33) Helander, M. G.; Wang, Z. B.; Mordoukhovski, L.; Lu, Z. H. *J. Appl. Phys.* **2008**, *104*, 094510.

(34) (a) Wang, Z. B.; Helander, M. G.; Greiner, M. T.; Qiu, J.; Lu, Z. H. *Appl. Phys. Lett.* **2009**, *95*, 043302. (b) Helander, M. G.; Greiner, M. T.; Wang, Z. B.; Lu, Z. H. *J. Appl. Phys.* **2009**, *106*, 056105.

(35) (a) Kulkarni, A. P.; Tonzola, C. J.; Babel, A.; Jenekhe, S. A. *Chem. Mater.* **2004**, *16*, 4556. (b) Hughes, G.; Bryce, M. R. *J. Mater. Chem.* **2005**, *15*, 94.

(36) Tang, C. W.; VanSlyke, S. A. *Appl. Phys. Lett.* **1987**, *51*, 913.

(37) Helander, M. G.; Wang, Z. B.; Lu, Z. H. *Appl. Phys. Lett.* **2008**, *93*, 083311.

AM1002603